In Situ Neutron Diffraction Study on Fast Oxide Ion Conductor $LaGaO_3$-Based Perovskite Compounds

Masahiro Kajitani,[†] Motohide Matsuda,[†] Akinori Hoshikawa,[‡] Stefanus Harjo,[‡] Takashi Kamiyama,[§] Toru Ishigaki,[||] Fujio Izumi,[⊥] and Michihiro Miyake*,[†]

Department of Environmental Chemistry and Materials, Faculty of Environmental Science and Technology, Okayama University, Okayama 700-8530, Japan, Japan Atomic Energy Research Institute, Tokai, Ibaraki 319-1195, Japan, Institute for Materials Structure Science, High Energy Accelerator Research Organization, Tukuba, Ibaraki, 305-0801, Japan, Department of Materials Science and Engineering, Muroran Institute of Technology, Muroran, Hokkaido 050-8585, Japan, and Advanced Materials Laboratory, National Institute for Materials Science, Tukuba, Ibaraki 305-0044, Japan

Received March 17, 2005. Revised Manuscript Received May 2, 2005

The crystal structures of $LaGaO_3$, $LaGa_{0.9}Mg_{0.1}O_{2.95}$, and $La_{0.9}Sr_{0.1}Ga_{0.9}Mg_{0.1}O_{2.9}$ have been investigated by high-temperature neutron powder diffraction in order to clarify a mechanism for high oxide ion conduction properties in $LaGaO_3$-based compounds. Parent phase $LaGaO_3$ crystallized in the orthorhombic (*Pbnm*) up to 150 °C and the rhombohedral ($R\bar{3}c$) at between 160 and 800 °C. $LaGa_{0.9}Mg_{0.1}O_{2.95}$ crystallized in the orthorhombic (*Ibmm*) up to 340 °C and the rhombohedral ($R\bar{3}c$) at between 350 and 800 °C. On the other hand, $La_{0.9}Sr_{0.1}Ga_{0.9}Mg_{0.1}O_{2.9}$ crystallized in the monoclinic ($I2/a$) up to 400 °C and the rhombohedral ($R\bar{3}c$) at between 410 and 800 °C. The correlations between the crystal structures and conduction properties of $LaGaO_3$-based materials were discussed on the basis of the analytical results.

Introduction

It is well-known that Sr- and Mg-doped $LaGaO_3$ (LSGM) perovskite is a superior oxide ion conductor.[1−7] The oxide ion conductivity of LSGM is much higher than that of conventional yttria-stabilized zirconia (YSZ). Furthermore, LSGM is almost a pure oxide ion conductor over a wide oxygen partial pressure range. Therefore, LSGM has attracted a great deal of attention as a solid electrolyte for lower-temperature-operating solid oxide fuel cells.[8−14]

Although several studies have been made on the crystal structure of LSGM,[15−19] little is known about the high oxide ion conduction mechanism of LSGM in detail. Furthermore, the effects of doping Sr and/or Mg in $LaGaO_3$-based systems have been investigated very little up to now. It is, therefore, of importance to systematically investigate these effects, and correlations between the crystal structures at high temperature and oxide ion conduction properties of $LaGaO_3$-based systems, because the oxide ion conduction property is strongly dependent upon the doping Sr and/or Mg. This investigation brings useful information to understanding the oxide ion conduction mechanism and designing a new oxide ion conductor with perovskite structure.

We have studied correlations between the crystal structures and oxide ion conduction properties of $LaGaO_3$-based compound systems such as parent phase $LaGaO_3$ (LG), Sr-doped $LaGaO_3$ (LSG), Mg-doped $LaGaO_3$ (LGM), and Sr- and Mg-doped $LaGaO_3$ (LSGM). We previously reported the crystal structures of these materials determined at room temperature by neutron powder diffraction.[20] In the present paper, we report the crystal structures at high temperatures

* Corresponding author. E-mail: mmiyake@cc.okayama-u.ac.jp. Fax: +81-86-251-8906.
[†] Okayama University.
[‡] Japan Atomic Energy Research Institute.
[§] High Energy Accelerator Research Organization.
[||] Muroran Institute of Technology.
[⊥] National Institute for Materials Science.

(1) Ishihara, T.; Matsuda, H.; Takita, Y. *J. Am. Chem. Soc.* **1994**, *116*, 3801.
(2) Feng, M.; Goodenough, J. B. *Eur. J. Solid State Inorg. Chem.* **1994**, *31*, 663.
(3) Ishihara, T.; Matsuda, H.; Takita, Y. *Solid State Ionics* **1995**, *79*, 147.
(4) Huang, K.; Feng, M.; Goodenough, J. B. *J. Am. Ceram. Soc.* **1996**, *79*, 1100.
(5) Huang, P.; Petric, A. *J. Electrochem. Soc.* **1996**, *143*, 1644.
(6) Huang, K.; Ticky, R. S.; Goodenough, J. B. *J. Am. Ceram. Soc.* **1998**, *81*, 2565.
(7) Huang, K.; Ticky, R. S.; Goodenough, J. B. *J. Am. Ceram. Soc.* **1998**, *81*, 2576.
(8) Huang, K.; Ticky, R. S.; Goodenough, J. B. *J. Am. Ceram. Soc.* **1998**, *81*, 2581.
(9) Feng, M.; Goodenough, J. B.; Huang, K.; Milliken, C. *J. Power Source* **1996**, *63*, 47.
(10) Ishihara, T.; Honda, M.; Shibayama, T.; Minami, H.; Nishiguchi, H.; Takita, Y. *J. Electrochem. Soc.* **1998**, *145*, 3177.
(11) Akikusa, J.; Adachi, K.; Hoshino, K.; Ishihara, T.; Takita, Y. *J. Electrochem. Soc.* **2001**, *148*, A1275.
(12) Yan, J. W.; Lu, Z. G.; Jiang, Y.; Dong, Y. L.; Yu, C. Y.; Li, W. Z. *J. Electrochem. Soc.* **2002**, *149*, A1132.
(13) Fukui, T.; Ohara, S.; Murata, K.; Yoshida, H.; Miura, K.; Inagaki, T. *J. Power Source* **2002**, *106*, 142.
(14) Matsuda, M.; Ohara, O.; Murata, K.; Ohara, S.; Fukui, T.; Miyake, M. *Electrochem. Solid State Lett.* **2003**, *6*, A140.
(15) Slater, P. R.; Irvine, J. T. S.; Ishihara, T.; Takita, Y. *J. Solid State Chem.* **1998**, *139*, 135.
(16) Slater, P. R.; Irvine, J. T. S.; Ishihara, T.; Takita, Y. *Solid State Ionics* **1998**, *107*, 319.
(17) Lerch, M.; Boysen, H.; Hansen, T. *J. Phys. Chem. Solids* **2001**, *62*, 445.
(18) Boysen, H.; Lerch, M.; Gilles, R.; Krimmer, B.; Tobbens, D. M. *Appl. Phys.* **2002**, *A74*, S966.
(19) Vasylechko, L.; Vashook, V.; Savytskii, D.; Senyshyn, A.; Niewa, R.; Knapp, M.; Ullmann, H.; Berkowski, M.; Matkovskii, A.; Bismayer, U. *J. Solid State Chem.* **2003**, *172*, 396.
(20) Kajitani, M.; Matsuda, M.; Hoshikawa, A.; Oikawa, K.; Torii, S.; Kamiyama, T.; Izumi, F.; Miyake, M. *Chem. Mater.* **2003**, *15*, 3468.

10.1021/cm050597n CCC: $30.25
Published on Web 07/15/2005

and the conduction mechanism of $LaGaO_3$-based materials where the concentrations of dopants are 10 mol % Sr on the La site and 10 mol % Mg on Ga site, based on neutron powder diffraction and oxide ion conductivity measurement. Neutron powder diffraction is a useful means for precisely determining the position and site occupancy of light elements such as oxygen atom in compounds containing heavy elements, and is helpful for comprehending the conduction mechanism of $LaGaO_3$-based perovskite compounds.

Experimental Section

Samples of $LaGaO_3$ (LG), $La_{0.9}Sr_{0.1}GaO_{2.95}$ (LSG91), $LaGa_{0.9}Mg_{0.1}O_{2.95}$ (LGM91), and $La_{0.9}Sr_{0.1}Ga_{0.9}Mg_{0.1}O_{2.9}$ (LSGM9191) were synthesized by conventional solid-state reactions. Powders of La_2O_3 (99.99%), $SrCO_3$ (99.9%), Ga_2O_3 (99.9%), and MgO (99.0%) were ball-milled for 24 h in ethanol with the appropriate stoichiometry. Before weighing, the La_2O_3 reagent was preheated at 1000 °C for 5 h in air to remove adsorbed water. The mixture obtained was then calcined at 1100 °C for 10 h in air. After the calcination, the mixture was sufficiently reground, pressed into pellets, and then sintered at 1300−1500 °C for 10 h in air. The product phase was confirmed by powder X-ray diffraction (XRD), using a Rigaku RINT2100/PC diffractometer with monochromated Cu Kα (λ = 1.5418 Å) radiation, and structural changes were, furthermore, examined by high-temperature XRD equipped with an electric furnace.

Time-of-flight (TOF) neutron powder diffraction data were collected at room temperature, 300, 500, and 800 °C using the 90 degree banks of the Sirius diffractometer[21] at KENS, High Energy Accelerator Research Organization (KEK), in Japan. The powdery samples were loaded in a cylindrical quartz cell under atmospheric pressure, and set on the diffractometer. The observed data as a function of time were converted into those as a function of *d* values, referring to intensity data observed in a separate measurement of Si powder as a standard sample. The collected diffraction data in a *d* range of 0.5 to 3.0 were analyzed by the Rietveld method using the program RIETAN-TN for TOF neutron powder diffraction.[22,23]

The impedance spectra of the sintered bodies were measured with a Hewlett-Packard 4192A impedance analyzer over a frequency range of 5 Hz to 13 MHz with an ac voltage of amplitude of 100 mV. Two electrodes were formed by coating platinum paste on both end surfaces of the samples and then fired at 1000 °C for 1 h in air.

Results and Discussion

XRD patterns showed that all the samples prepared here were single phases except the LSG91 sample. LSG91 samples coexisted with a small amount of $LaSrGa_3O_7$ as an impurity phase despite repeated heat treatments. Sr was not easily doped in the La site of LG, whereas it was easily doped in that of LGM91. Matraszek et al.[24] reported that maximum solid solubility of Sr in $LaGaO_3$ is about 2 mol %. This supports our results.

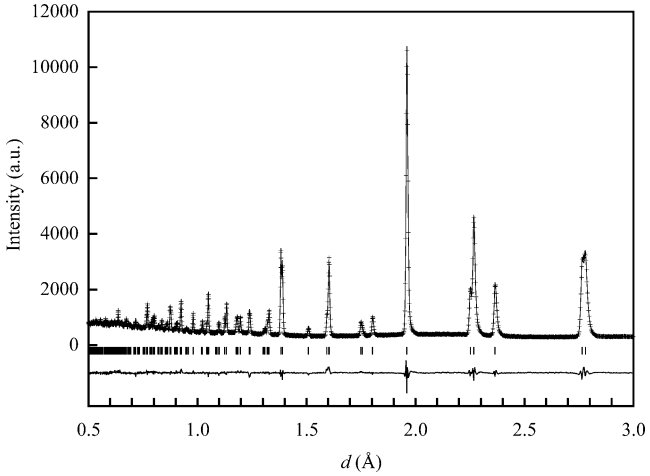

Figure 1. Observed (plus signs), calculated (solid line), and difference (solid line on the bottom) patterns for TOF neutron powder diffraction data on $LaGaO_3$ at 800 °C.

The structural data at room temperature by Kajitani et al.[20] and at high temperature by Marti et al.,[25] Howard et al.,[26] and Slater et al.[15,16] were adopted as initial parameters. Structure refinements were performed on applying anisotropic displacement parameters for oxygen sites, because $LaGaO_3$-based materials are oxide ion conductors. The parent phase, LG, crystallized in the orthorhombic with space group *Pbnm* at room temperature, and underwent a phase transition from the orthorhombic to the rhombohedral at 150−160 °C, as previously reported.[15−19] Arguments were divided as to the space group of high-temperature phase of LG, i.e., *R*3*c* or $R\bar{3}c$.[25,26] The differences between two space groups are mainly the *z* fractional coordinates of La, Ga, and O atoms. For example, the Ga atom is at the 6a (0, 0, *z*) special position in the space group *R*3*c* with noncentrosymmetry, while it is at the 6b (0, 0, 0) special position in the space group $R\bar{3}c$ with centrosymmetry. In the refinements at 300 °C based on *R*3*c*, the *z* fractional coordinate of Ga atom was converged to $z = 0.0000(8)$. This was regarded as the Ga atom existing at the 6b (0, 0, 0) special position in the space group $R\bar{3}c$. The *z* fractional coordinates of La and O atoms in the space group *R*3*c* were also approached to those of La and O atoms in the space group $R\bar{3}c$. Consequently, $R\bar{3}c$ rather than *R*3*c* was adopted as the space group of LG at 300 °C. The same results were observed in the temperature range of 500−800 °C, and the *R* factors based on the space group $R\bar{3}c$ showed good fit. Figure 1 shows the observed, calculated, and difference patterns for LG at 800 °C. The final structural parameters and *R* factors of LG at room temperature, 300, 500, and 800 °C are summarized in Table 1. The refined structural parameters of LG at high temperatures were consistent with those of previous reports.[17,26]

In the refinements of LGM91 and LSGM9191, the site occupancies of the La and/or Ga atoms were fixed according to the chemical composition, and the positional and thermal parameters for the Sr and Mg atoms were reset by those for the La and Ga atoms, respectively, because the site occupan-

(21) Kamiyama, T.; Torii, S.; Mori, K.; Oikawa, K.; Itoh, S.; Furusaka, M.; Satoh, S.; Egami, T.; Ikeda, T.; Izumi, F.; Asano, H. *Mater. Sci. Forum* **2000**, *321*−*324*, 302.
(22) Ohta, T.; Izumi, F.; Oikawa, K.; Kamiyama, T. *Physica B* **1997**, *234*−*236*, 1093.
(23) Izumi, F.; Ikeda, T. *Mater. Sci. Forum* **2000**, *321*−*324*, 198.
(24) Matraszek, A.; Singheiser, L.; Kobertz, D.; Hilpert, K.; Miller, M.; Schulz, O.; Martin, M. *Solid State Ionics* **2004**, *166*, 343.
(25) Marti, W.; Fischer, P.; Altorfer, F.; Scheel, H. J.; Tadin, M. J. *J. Phys. Condens. Matter* **1994**, *6*, 127.
(26) Howard, C. J.; Kennedy, B. J. *J. Phys. Condens. Matter* **1999**, *11*, 3229.

Table 1. Final Structural Parameters and *R* Factors[a] of $LaGaO_3$ at Room Temperature, 300, 500, and 800 °C

	RT	300 °C	500 °C	800 °C
structure	orthorhombic	rhombohedral	rhombohedral	rhombohedral
space group	*Pbnm*	*R*$\bar{3}$*c*	*R*$\bar{3}$*c*	*R*$\bar{3}$*c*
a (Å)	5.5272(2)	5.5370(1)	5.5465(1)	5.5597(1)
b (Å)	5.4943(1)			
c (Å)	7.7781(3)	13.4035(3)	13.4473(2)	13.5089(3)
V (Å^3)	236.20(2)	355.87(1)	358.27(1)	361.62(1)
		atom La		
site	4*c*	6*a*	6*a*	6*a*
g	1.0	1.0	1.0	1.0
x	−0.0045(4)	0	0	0
y	−0.0165(3)	0	0	0
z	1/4	1/4	1/4	1/4
U (Å^2)	0.0047(2)	0.0081(2)	0.0120(2)	0.0180(3)
		atom Ga		
site	4*b*	6*b*	6*b*	6*b*
g	1.0	1.0	1.0	1.0
x	1/2	0	0	0
y	0	0	0	0
z	0	0	0	0
U (Å^2)	0.0047(2)	0.0070(2)	0.0080(2)	0.0125(3)
		atom O1		
site	4*c*	18*e*	18*e*	18*e*
g	1.0	1.0	1.0	1.0
x	0.0677(4)	0.5561(1)	0.5546(1)	0.5523(1)
y	0.5066(6)	0	0	0
z	1/4	1/4	1/4	1/4
U (Å^2)	0.007	0.013	0.017	0.026
U_{11} (Å^2)	0.0059(1)	0.011(3)	0.016(1)	0.022(1)
U_{22} (Å^2)	0.0015(1)	0.010(4)	0.013(1)	0.019(1)
U_{33} (Å^2)	0.013(1)	0.015(1)	0.020(1)	0.0031(1)
U_{12} (Å^2)	0.0002(13)	1/2*U*22	1/2*U*22	1/2*U*22
U_{13} (Å^2)	0	−0.0063(4)	−0.0049(1)	−0.0020(1)
U_{23} (Å^2)	0	2*U*13	2*U*13	2*U*13
		atom O2		
site	8*d*			
g	1.0			
x	−0.2307(3)			
y	0.2304(3)			
z	0.0356(2)			
U (Å^2)	0.008			
U_{11} (Å^2)	0.0081(8)			
U_{22} (Å^2)	0.0074(9)			
U_{33} (Å^2)	0.0071(8)			
U_{12} (Å^2)	0.0033(1)			
U_{13} (Å^2)	0.021(14)			
U_{23} (Å^2)	−0.0018(1)			
R_{wp}	0.0350	0.0332	0.0341	0.0354
R_p	0.0289	0.0282	0.0272	0.0277
R_I	0.0253	0.0201	0.0183	0.0212
R_F	0.0197	0.0198	0.0187	0.0344
S	1.49	1.40	1.50	1.80

[a] $R_{wp} = [(\sum_i w_i\{y_i - f_i(x)\}^2)/\sum_i w_i y_i^2)]^{1/2}$, $R_p = (\sum_i |y_i - f_i(x)|)/\sum_i y_i)$, $R_B = (\sum_k |I_k(\text{“}o\text{”}) - I_k(c)|/\sum_k I_k(\text{“}o\text{”}))$. $R_F = (\sum_k |F_k(\text{“}o\text{”})| - |F_k|/\sum_k |F_k(\text{“}o\text{”})|)$, $S = (R_{wp}/R_e)$. $B = 8\pi^2 U$. $U = \exp\{-2\pi^2(h^2a^{*2}U_{11} + k^2b^{*2}U_{22} + l^2c^{*2}U_{33} + 2hka^*b^*U_{12} + 2hla^*c^*U_{13} + 2klb^*c^*U_{23})\}$.

cies approached the values expected from the chemical composition when they were refined. The site occupancies of oxygen atoms were refined in order to determine the oxygen vacancy sites and concentration.

Powder XRD patterns of LG and LGM91 at room temperature are shown in Figure 2. Some reflections, e.g., 111 reflection, derived from the orthorhombic with space group *Pbnm* were not observed on the XRD pattern of LGM91. According to the extinction rule, 111 reflection is allowed in the orthorhombic primitive lattice, whereas it is forbidden in the orthorhombic body-centered lattice. Namely, this suggests the symmetry of LGM91 belongs to the

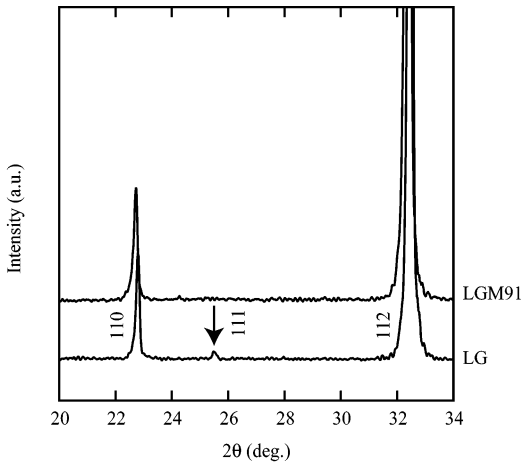

Figure 2. Comparison between power XRD patterns of $LaGaO_3$ and $LaGa_{0.9}Mg_{0.1}O_{2.95}$ at room temperature.

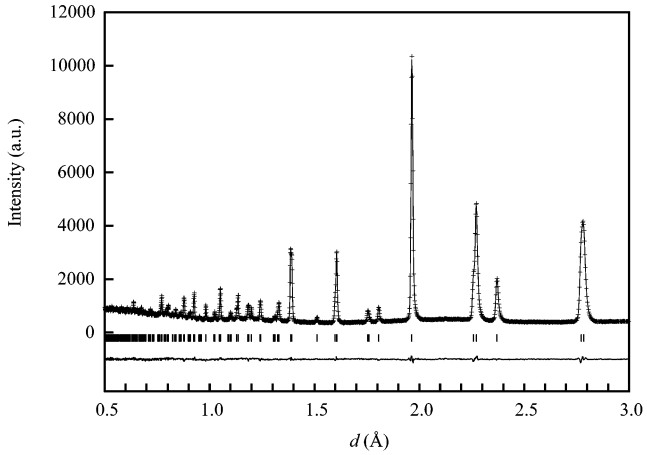

Figure 3. Observed (plus signs), calculated (solid line), and difference (solid line on the bottom) patterns for TOF neutron powder diffraction data on $LaGa_{0.9}Mg_{0.1}O_{2.95}$ at 800 °C.

orthorhombic body-centered lattice, as reported by Shibasaki et al.[27] Structure refinement at room-temperature based on the space group *Ibmm*[17] brought a good fit ($R_{wp} = 0.0357$). Consequently, LGM91 was found to crystallize in the orthorhombic with the space group *Ibmm* at room temperature. The high-temperature XRD revealed that LGM91 underwent a phase transition from the orthorhombic to the rhombohedral at 340−350 °C. The doping Mg in LG phase significantly made the transition temperature rise, compared with the parent phase LG. The neutron powder diffraction patterns of LGM91 collected at 500 and 800 °C were refined, using two possible space groups: *R*3*c* and *R*$\bar{3}$*c*. In the refinements at 500 and 800 °C based on *R*3*c*, the *z* fractional coordinates of La, Ga, and O atoms approached those based on *R*$\bar{3}$*c*, as observed for the refinements of LG in the temperature range of 300−800 °C. As a result, it was found that LGM91 at 500 and 800 °C crystallized in the rhombohedral space group *R*$\bar{3}$*c* and the *R* factors based on the space group *R*$\bar{3}$*c* converged with good fit (see Figure 3). The final structural parameters and *R* factors of LGM91 at room temperature, 300, 500, and 800 °C are listed in Table 2. The

(27) Shibasaki, T.; Furuya, T.; Wang, S.; Hashimoto, T. *Solid State Ionics* **2004**, *174*, 193.

Table 2. Final Structural Parameters and *R* Factors of $LaGa_{0.9}Mg_{0.1}O_{2.95}$ at Room Temperature, 300, 500, and 800 °C

	RT	300 °C	500 °C	800 °C
structure	orthorhombic	orthorhombic	rhombohedral	rhombohedral
space group	*Ibmm*	*Ibmm*	$R\bar{3}c$	$R\bar{3}c$
a (Å)	5.5361(2)	5.5094(2)	5.5502(2)	5.5689(2)
b (Å)	5.4981(2)	7.8098(3)		
c (Å)	7.7932(3)	5.5476(2)	13.4942(3)	13.5532(3)
V (Å^3)	237.21(2)	238.70(1)	359.99(2)	364.01(2)
atom			La	
site	4*e*	4*e*	6*a*	6*a*
g	1.0	1.0	1.0	1.0
x	0.4960(5)	0.4971(5)	0	0
y	0	0	0	0
z	3/4	3/4	1/4	1/4
U (Å^2)	0.0101(3)	0.0131(3)	0.0147(4)	0.0198(3)
atom			Ga/Mg	
site	4*a*	4*a*	6*a*	6*a*
g	0.9/0.1	0.9/0.1	0.9/0.1	0.9/0.1
x	0	0	0	0
y	0	0	0	0
z	0	0	0	0
U (Å^2)	0.0051 (3)	0.0067(3)	0.0102(4)	0.0135(3)
atom			O1	
site	4*e*	4*e*	18*e*	18*e*
g	1.02(1)	1.01(1)	0.979(4)	0.979(4)
x	0.0634(6)	0.0613(6)	0.5524(1)	0.5490(1)
y	0	0	0	0
z	1/4	1/4	1/4	1/4
U (Å^2)	0.009	0.012	0.023	0.031
U_{11} (Å^2)	0.0095(16)	0.012(1)	0.020(1)	0.030(1)
U_{22} (Å^2)	0.010(2)	0.012(2)	0.016(1)	0.026(1)
U_{33} (Å^2)	0.0056(26)	0.013(3)	0.032(1)	0.037(1)
U_{12} (Å^2)	0	0	1/2*U*22	1/2*U*22
U_{13} (Å^2)	0	0	−0.0068(9)	−0.0092(1)
U_{23} (Å^2)	0	0	2*U*13	2*U*13
atom			O2	
site	8*g*	8*g*		
g	0.95(1)	0.958(6)		
x	3/4	3/4		
y	1/4	1/4		
z	0.0352(3)	0.0347(3)		
U (Å^2)	0.022	0.025		
U_{11} (Å^2)	0.033(3)	0.023(3)		
U_{22} (Å^2)	0.027(2)	0.028(1)		
U_{33} (Å^2)	0.0054(12)	0.015(4)		
U_{12} (Å^2)	0	0		
U_{13} (Å^2)	0	0		
U_{23} (Å^2)	0.023(1)	0.024(1)		
R_{wp}	0.0356	0.0343	0.0370	0.0288
R_p	0.0309	0.0292	0.0316	0.0246
R_I	0.0382	0.0354	0.0337	0.0302
R_F	0.0370	0.0357	0.0433	0.0452
S	1.50	1.56	1.72	1.55

doping Mg in LG led the cell volume to the expansion. This is consistent with the expectation based on ionic radius.[28]

Several studies have been made on the crystal structure of LSGM by neutron powder diffraction[15−20] and Raman spectroscopy.[29−31] The crystal structures of LSGM systems have been strongly dependent upon the doped Sr and/or Mg contents. Namely, Slater et al.,[15,16] Boysen et al.,[18] and Vasylechko et al.[19] reported that $La_{0.9}Sr_{0.1}Ga_{0.8}Mg_{0.2}O_{2.85}$ (LSGM9182) crystallized in the monoclinic with space group *I*2/*a*, while Kajitani et al.[20] reported that $La_{0.8}Sr_{0.2}Ga_{0.8}Mg_{0.2}O_{2.8}$ (LSGM8282) crystallized in the cubic with space group $Pm\bar{3}m$, which is an ideal perovskite structure, i.e., the prototype structure. The structure refinements of LSGM9191 were examined, using four space groups as follows: *Pbnm* (orthorhombic),[3] *Ibmm* (orthorhombic),[17] *I*2/*a* (monoclinic), and $Pm\bar{3}m$ (cubic). The comparison among the results of refinements based on four space groups suggested that the crystal structure of LSGM9191 prepared here belonged to the monoclinic (*I*2/*a*), isostructural with LSGM9182 at room temperature. The monoclinic angles ($\beta = 90.07(1)°$) were observed at between room temperature and 300 °C and the *R* factor based on the monoclinic (*I*2/*a*) converged with the best fit.

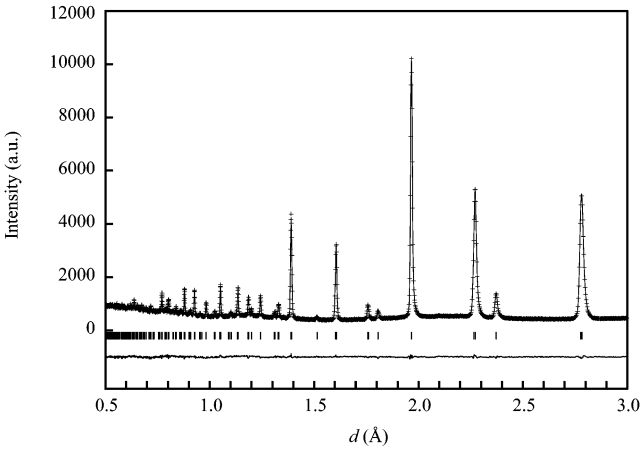

Figure 4. Observed (plus signs), calculated (solid line), and difference (solid line on the bottom) patterns for TOF neutron powder diffraction data on $La_{0.9}Sr_{0.1}Ga_{0.9}Mg_{0.1}O_{2.9}$ at 800 °C.

The high-temperature XRD revealed that the symmetry of LSGM9191 lattice ascended from the monoclinic to the rhombohedral at 400−410 °C. The doping Sr in LGM91 furthermore made the transition temperature rise. Thus, the crystal structure of LSGM9191 at 300 °C was analyzed in the monoclinic with space group *I*2/*a*. The neutron powder diffraction patterns of LSGM9191 collected at 500 and 800 °C were refined, using two possible space groups: *R*3*c* and $R\bar{3}c$. In the refinements at 500 and 800 °C, no significant differences between the *z* fractional coordinates based on *R*3*c* and $R\bar{3}c$ were observed, in a manner similar to the refinements of high-temperature phase in LG and LGM91. It was, therefore, decided that the correct space group of LSGM9191 at 500 and 800 °C was $R\bar{3}c$ rather than *R*3*c*, and the *R* factors based on the space group $R\bar{3}c$ converged with good fit (see Figure 4). The final structural parameters and *R* factors of LSGM9191 at room temperature, 300, 500, and 800 °C are listed in Table 3. The monoclinic angles ($\beta = 90.07(1)°$) observed at room temperature were hardly altered up to the transition temperature. The doping Sr in LGM91 led the cell volume to the expansion, corresponding to Sr^{2+} ion larger than La^{3+} ion in ionic radius.[28]

The selected bond lengths in LG, LGM91, and LSGM9191 are listed in Table 4, and the mean La−O and Ga−O bond lengths in LG, LGM91, and LSGM9191 as a function of temperature are shown in Figure 5. The mean La−O bond

(28) Shannon, R. D. *Acta Crystallogr.* **1967**, *A32*, 751.
(29) Sammes, N. M.; Tompsett, G. A.; Phillips, R. J.; Cartner, A. M. *Solid State Ionics* **1998**, *111*, 1.
(30) Yao, W.; Tang, Z.; Zhang, Z.; Luo, S.; Li, J.; Tan, Q. *Mater. Sci. Eng.* **2003**, *B99*, 309.
(31) Shkerin, S. N.; Bronin, D. I.; Kovyazina, S. A.; Gorelov, V. P.; Kuzmin, A. V.; Martemyanova, Z. S.; Beresnev, S. M. *Solid State Ionics* **2004**, *171*, 129.

Table 3. Final Structural Parameters and *R* Factors of $La_{0.9}Sr_{0.1}Ga_{0.9}Mg_{0.1}O_{2.9}$ at Room Temperature, 300, 500, and 800 °C

	RT	300 °C	500 °C	800 °C
structure	monoclinic	monoclinic	rhombohedral	rhombohedral
space group	*I*2/*a*	*I*2/*a*	$R\bar{3}c$	$R\bar{3}c$
a (Å)	7.8120 (4)	7.8189(4)	5.5510(2)	5.5684(2)
b (Å)	5.5420(3)	5.5455(3)		
c (Å)	5.5121(3)	5.5184(3)	13.5305(5)	13.5904(5)
β (°)	90.07(1)	90.07(1)		
V (Å^3)	238.64(2)	239.28(2)	361.07(2)	364.94(2)
		atom La/Sr		
site	4*e*	4*e*	6*a*	6*a*
g	0.9/0.1	0.9/0.1	0.9/0.1	0.9/0.1
x	1/4	1/4	0	0
y	−0.0023 (8)	−0.0016 (7)	0	0
z	0	0	1/4	1/4
U (Å^2)	0.0114(4)	0.0144(4)	0.0189(3)	0.0225(3)
		atom Ga/Mg		
site	4*b*	4*b*	6*a*	6*a*
g	0.9/0.1	0.9/0.1	0.9/0.1	0.9/0.1
x	0	0	0	0
y	1/2	1/2	0	0
z	0	0	0	0
U (Å^2)	0.0063(4)	0.0081(3)	0.0112(3)	0.0133(3)
		atom O1		
site	4*e*	4*e*	18*e*	18*e*
g	1.01(2)	1.00(2)	0.959(2)	0.965(2)
x	1/4	1/4	0.5440(2)	0.5384(2)
y	0.4418(10)	0.4473(9)	0	0
z	0	0	1/4	1/4
U (Å^2)	0.011	0.019	0.031	0.039
U_{11} (Å^2)	0.012(4)	0.023(4)	0.032(1)	0.042(1)
U_{22} (Å^2)	0.007(2)	0.007(2)	0.026(1)	0.034(1)
U_{33} (Å^2)	0.015(4)	0.028(5)	0.033(1)	0.040(1)
U_{12} (Å^2)	0	0	1/2*U*22	1/2*U*22
U_{13} (Å^2)	0.003(7)	−0.023(4)	−0.0096(4)	−0.013(1)
U_{23} (Å^2)	0	0	2*U*13	2*U*13
		atom O2		
site	8*f*	8*f*		
g	0.92(1)	0.95(1)		
x	0.4695(6)	0.4704(6)		
y	0.764(2)	0.747(3)		
z	0.230 (2)	0.247(2)		
U (Å^2)	0.028	0.035		
U_{11} (Å^2)	0.021(3)	0.030(3)		
U_{22} (Å^2)	0.036(3)	0.040(3)		
U_{33} (Å^2)	0.025(2)	0.034(3)		
U_{12} (Å^2)	−0.015(5)	0.018(4)		
U_{13} (Å^2)	0.0004(5)	−0.018(3)		
U_{23} (Å^2)	−0.031(2)	−0.038(2)		
R_{wp}	0.0405	0.0322	0.0339	0.0284
R_p	0.0347	0.0275	0.0288	0.0245
R_I	0.0684	0.0404	0.0359	0.0338
R_F	0.0742	0.0455	0.0540	0.0529
S	2.21	1.63	1.62	1.56

lengths in LG dramatically elongated up to 300 °C, and after that, they monotonically increased, while those in the doped samples were approximately equal to each other and monotonically increased with increasing temperature. On the other hand, the mean Ga−O bond lengths in LGM91 were monotonically elongated with increasing temperature, whereas those in LG and LSGM9191 were lengthened with increasing temperature beyond 300 °C, after shrinkage. The mean Ga−O bond lengths in LSGM9191 were shorter than those in LG and LGM91, although the unit cell volume is the largest in these systems. In La−O bond lengths, the deviations from the mean La−O bond lengths were decreased with increasing temperature as seen in Table 4, that is, the LaO_{12} polyhedron was close to a regular one with increasing temperature. The Ga−O bond lengths in all the low-temperature phases were slightly elongated along the direction of the apical O1 site, whereas the GaO_6 octahedra were regular in all the high-temperature phases.

The GaO_6 octahedral tilts in all the samples are discussed from the standpoints of both the mean bond lengths and tolerance factor. In general, $LaGaO_3$-based material has a distortion from an ideal perovskite-type structure, i.e., primitive structure with the cubic symmetry, and the distortion is caused by the GaO_6 octahedral tilts.[15−20,25,26] The GaO_6 octahedral tilts were observed in all the samples up to 800 °C. Figure 6 shows the schematic structural models of LG, LGM91, and LSGM9191 at room temperature. In LG with the orthorhombic (*Pbnm*), there are two tilt directions observed around the *b* (//[110]p) and *c* (//[001]p) axes, and represented as $a^+b^-b^-$, according to Glazer's notation[32] that proposed a classification of the distortion caused by octahedral tilts in perovskite structure. In LGM91 with the orthorhombic (*Ibmm*), there are two tilt directions observed around the *b* (//$[110]_p$) and *c* (//$[001]_p$) axes, and represented as $a^0b^-b^-$. On the other hand, in LSGM9191 with the monoclinic (*I*2/*a*) the tilts occurred around the *a* (//$[001]_p$) and *c* (//$[110]_p$) axes and can be described as $a^-b^-b^-$. These tilts around the axes became equal in the high-temperature forms, because the oxygen atom sites are equivalent in the rhombohedral ($R\bar{3}c$), and are represented as $a^-a^-a^-$. Figure 7 shows GaO_6 octahedral tilt angles for LG, LGM91, and LSGM9191 as a function of temperature. Their octahedral tilt angles were calculated using the lattice parameters and the positional parameters. The GaO_6 octahedral tilts in all the samples were reduced with increasing temperature. Compared with LG structure, the GaO_6 octahedral tilts in LGM91 were reduced by doping Mg in LG. Furthermore, doping Sr in LGM91 led to the reduction of GaO_6 octahedral tilts. Namely, the doping Sr and/or Mg significantly affected the GaO_6 octahedral tilts. The GaO_6 octahedral tilts in LSGM9191 were prominently reduced in the temperature range 500−800 °C, although the lattice has the same symmetry as high-temperature phases of LG and LGM91.

It is well-known that the tolerance factor, *t*, is a relevant parameter for estimating the magnitude of distortion in a ABO_3 perovskite structure.[33] The tolerance factor is represented by

$$t = \frac{d_{AO}}{\sqrt{2}d_{BO}}$$

where d_{AO} and d_{BO} are mean A−O and B−O bond lengths, respectively. When the tolerance factor is close to unity, the distortion is reduced, and the perovskite structure gets closer to the cubic. The tolerance factors of LSGM9191 at high temperatures (500−800 °C) were closer to unity than those of LG and LGM91 at high temperatures (500−800 °C) as shown in Table 4, because the mean Ga−O bond lengths of LSGM9191 were shortened by doping Sr in LGM91, compared with those of LG and LGM91 (cf. Figure 5). This

(32) Glazer, A. M. *Acta Crystallogr*. **1975**, *A31*, 756.
(33) Goldschmidt, V. M. Geochemische Vertcitunhsgesetze der Elemente VII, VIII, 1927/28.

Table 4. Selected Bond Lengths (Å) and Tolerance Factors (*t*) of $LaGaO_3$, $LaGa_{0.9}Mg_{0.1}O_{2.95}$, and $La_{0.9}Sr_{0.1}Ga_{0.9}Mg_{0.1}O_{2.9}$ at Room Temperature, 300, 500, and 800 °C

	RT	300 °C	500 °C	800 °C
		$LaGaO_3$		
structure	orthorhombic	rhombohedral	rhombohedral	rhombohedral
space group	*Pbnm*	*R*$\bar{3}$*c*	*R*$\bar{3}$*c*	*R*$\bar{3}$*c*
La−O1	2.418(3) (×2)	2.4586(6) (×3)	2.4660(7) (×3)	2.4890(8) (×3)
La−O1	2.650(3) (×2)	2.7643(1) (×6)	2.7715(1) (×6)	2.7802(1) (×6)
La−O1	2.902(3) (×2)	3.0783(6) (×3)	3.0804(7) (×3)	3.0707(8) (×3)
La−O2	2.487(2) (×2)			
La−O2	2.619(2) (×2)			
La−O2	2.830(2) (×2)			
mean La−O	2.651	2.766	2.772	2.780
Ga−O1	1.981(1) (×2)	1.9744(1) (×6)	1.9783(1) (×6)	1.9818(1) (×6)
Ga−O2	1.973(2) (×2)			
Ga−O2	1.974(2) (×2)			
mean Ga−O	1.976	1.974	1.978	1.982
t	0.949	0.991	0.991	0.992
		$LaGa_{0.9}Mg_{0.1}O_{2.95}$		
structure	orthorhombic	orthorhombic	rhombohedral	rhombohedral
space group	*Ibmm*	*Ibmm*	*R*$\bar{3}$*c*	*R*$\bar{3}$*c*
La−O1	2.443(4) (×1)	2.450(4) (×1)	2.4842(8) (×3)	2.5117(7) (×3)
La−O1	2.774(1) (×2)	2.778(1) (×2)	2.7767(1) (×6)	2.7859(1) (×6)
La−O1	3.093 (4) (×1)	3.098(4) (×1)	3.0660(8) (×3)	3.0572(7) (×3)
La−O2	2.558(2) (×4)	2.570(2) (×4)		
La−O2	2.968(2) (×4)	2.968(2) (×4)		
mean La−O	2.766	2.771	2.776	2.785
Ga−O1	1.979(1) (×2)	1.982(1) (×2)	1.9789(1) (×6)	1.9835(1) (×6)
Ga−O2	1.970(1) (×4)	1.973(1) (×4)		
mean Ga−O	1.973	1.976	1.979	1.984
t	0.991	0.992	0.992	0.993
		$La_{0.9}Sr_{0.1}Ga_{0.9}Mg_{0.1}O_{2.9}$		
structure	monoclinic	monoclinic	rhombohedral	rhombohedral
space group	*I2/a*	*I2/a*	*R*$\bar{3}$*c*	*R*$\bar{3}$*c*
La−O1	2.450 (7) (×1)	2.479(7) (×1)	2.5313(9) (×3)	2.5702(8) (×3)
La−O1	2.775 (1) (×2)	2.775(1) (×2)	2.7772(1) (×6)	2.7857(1) (×6)
La−O1	3.093 (7) (×1)	3.067(7) (×1)	3.0198(9) (×3)	2.9982(8) (×3)
La−O2	2.523 (7) (×2)	2.589(11) (×2)		
La−O2	2.677(14) (×2)	2.628(18) (×2)		
La−O2	2.870(13) (×2)	2.916(16) (×2)		
La−O2	3.004(6) (×2)	2.964(10) (×2)		
mean La−O	2.770	2.774	2.776	2.785
Ga−O1	1.980(1) (×2)	1.9771(9) (×2)	1.9745(1) (×6)	1.9780(1) (×6)
Ga−O2	1.965(11) (×2)	1.968(18) (×2)		
Ga−O2	1.977(12) (×2)	1.970(18) (×2)		
mean Ga−O	1.974	1.972	1.975	1.978
t	0.992	0.995	0.994	0.996

corresponds to the fact that the GaO_6 octahedral tilts in LSGM9191 were significantly reduced. In addition, we previously reported that LSGM8282 crystallized in the cubic exhibited no tilts, and the mean Ga−O bond lengths were shorter than those of $LaGa_{0.8}Mg_{0.2}O_{2.9}$ (LGM82) with the orthorhombic.[20] These suggest that shortening the mean Ga−O bond lengths by doping Sr is much effective for the reduction of the GaO_6 octahedral tilts.

Figure 8 shows the temperature dependences of conductivities of LGM91 and LSGM9191. The conductivity of LSGM9191 was higher than that of LGM91 over the measured temperature range. The slopes of the curves were changed at about 500 and 440 °C for LGM91 and LSGM9191, respectively. Activation energies for conduction of LGM91 estimated from the Arrhenius plot of conductivities were about 0.70 eV in the temperature range 900−500 °C and about 1.19 eV in the temperature range 500−300 °C, respectively. On the other hand, those of LSGM9191 were about 0.53 eV in the temperature range 900−440 °C and about 1.11 eV in the temperature range 440−300 °C. The activation energies for conduction in LSGM9191 were lower than those of LGM91 over the measured temperature range.

The oxygen site occupancies in LGM91 and LSGM9191 were in good agreement with the stoichiometric proportions over the measured temperature range. The oxygen vacancies in LGM91 with the orthorhombic were preferentially created at the planar O2 site of the GaO_6 octahedron, whereas the apical O1 site of the GaO_6 octahedron was fully occupied as shown in Table 2. In LGM91 with the rhombohedral, the oxygen vacancies were in disorder, because all oxygen atom sites were equivalent. The oxygen vacancies in LSGM9191 with the monoclinic were also preferentially created at the planar O2 site of the GaO_6 octahedron, whereas the apical O1 site of the GaO_6 octahedron was fully occupied as shown in Table 3. In LSGM9191 with the rhombohedral, oxygen vacancies were in disorder, similar to the high-temperature phase of LGM91.

The oxide ion conduction properties are predicted to be closely related to the anisotropic displacement parameters

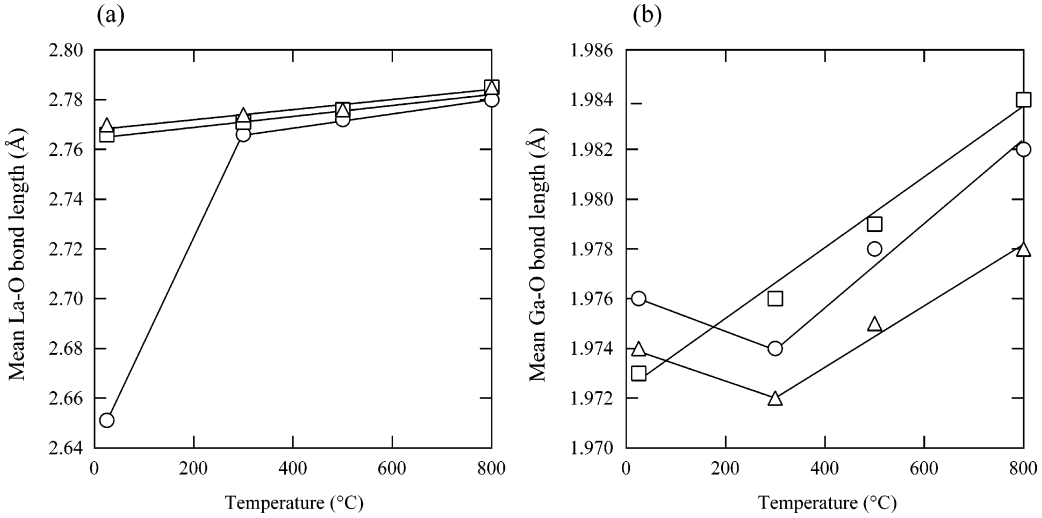

Figure 5. (a) Mean La−O bond lengths and (b) Ga−O bond lengths of $LaGaO_3$ (open circle), $LaGa_{0.9}Mg_{0.1}O_{2.95}$ (open square), and $La_{0.9}Sr_{0.1}Ga_{0.9}Mg_{0.1}O_{2.9}$ (open triangle) as a function of temperature.

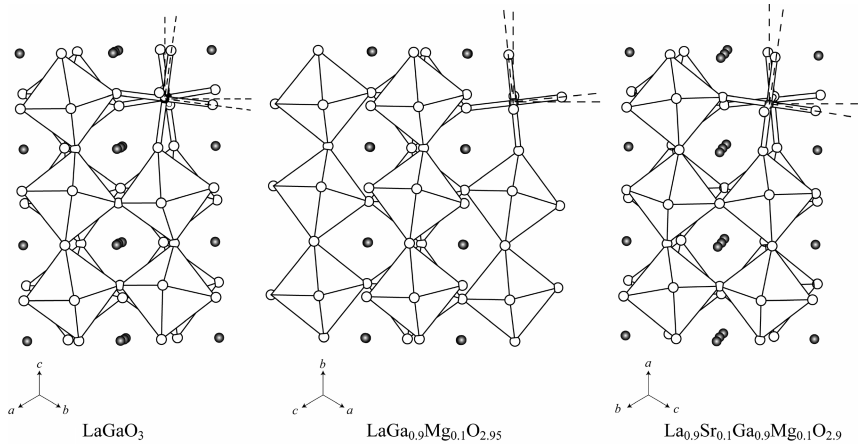

Figure 6. Structural models of $LaGaO_3$, $LaGa_{0.9}Mg_{0.1}O_{2.95}$, and $La_{0.9}Sr_{0.1}Ga_{0.9}Mg_{0.1}O_{2.9}$ at room temperature. The broken line represents the GaO_6 octahedral tilt angles.

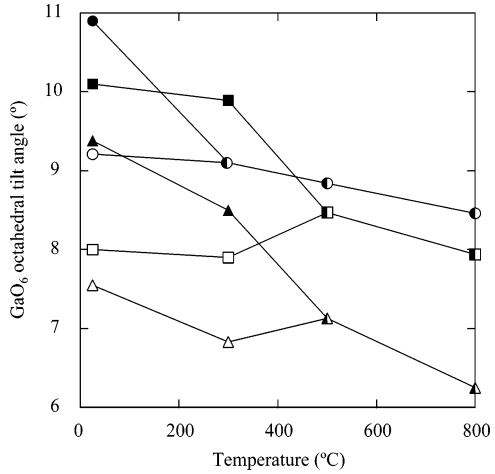

Figure 7. GaO_6 octahedral tilt angles of $LaGaO_3$ (circle), $LaGa_{0.9}Mg_{0.1}O_{2.95}$ (square), and $La_{0.9}Sr_{0.1}Ga_{0.9}Mg_{0.1}O_{2.9}$ (triangle) as a function of temperature. Open, filled, and half-filled symbols represent tilt angles around the $[110]_p$, $[001]_p$, and $[111]_p$, respectively, of primitive perovskite lattice.

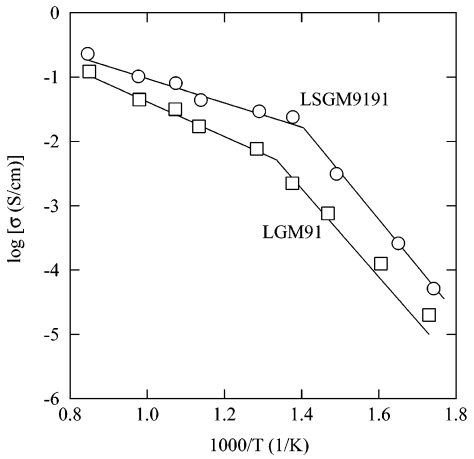

Figure 8. Temperature dependences of conductivities of $LaGa_{0.9}Mg_{0.1}O_{2.95}$ (open square) and $La_{0.9}Sr_{0.1}Ga_{0.9}Mg_{0.1}O_{2.9}$ (open circle).

for oxygen sites and the mean O−O interatomic distances. The oxide ions in LGM91 and LSGM9191 up to 300 °C were localized and showed a small ellipsoid. Then, the displacement of the oxide ions in LGM91 and LSGM9191 were spread toward the neighboring oxygen site by the symmetry of lattice changing to the rhombohedral. Figure 9 shows views of the GaO_6 octahedra of LG, LGM91, and LSGM9191 at 800 °C. The oxide ion in LSGM9191 showed a larger anisotropic distribution than that in LG and LGM91 at all temperature ranges, although the GaO_6 octahedral tilt angles for LSGM9191 were the smallest in all the samples.

In addition, the interatomic distances between oxygen atoms of LSGM9191 were shorter than those of LGM91, as

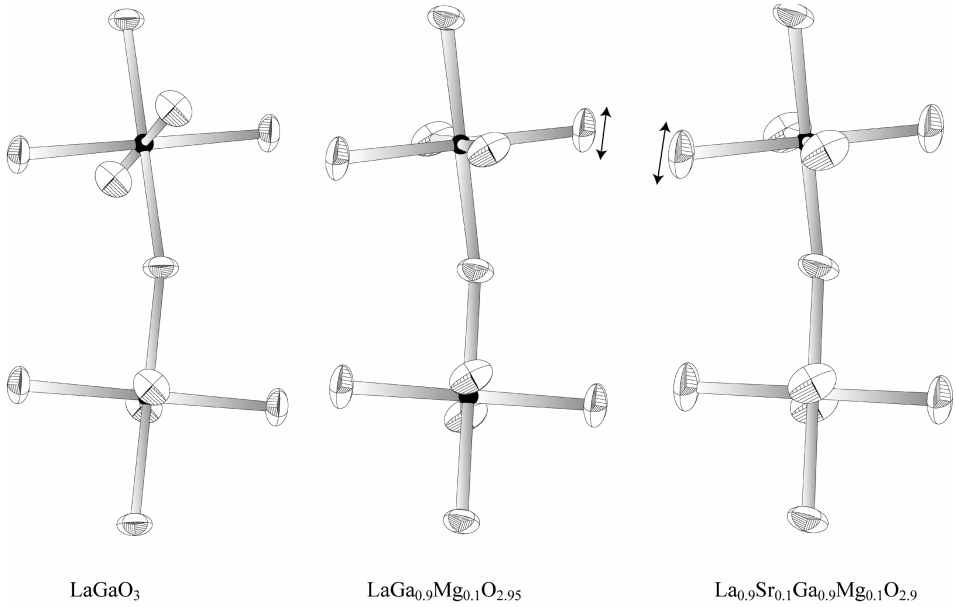

Figure 9. Views of the GaO_6 octahedra in $LaGaO_3$, $LaGa_{0.9}Mg_{0.1}O_{2.95}$, and $La_{0.9}Sr_{0.1}Ga_{0.9}Mg_{0.1}O_{2.9}$ at 800 °C.

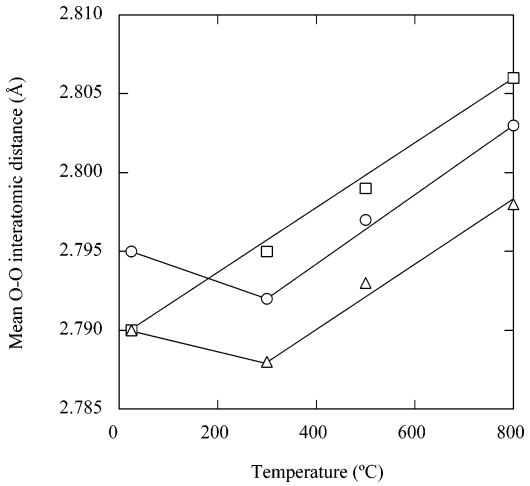

Figure 10. Temperature dependences of the mean O−O interatomic distances of $LaGaO_3$ (open circle), $LaGa_{0.9}Mg_{0.1}O_{2.95}$ (open square), and $La_{0.9}Sr_{0.1}Ga_{0.9}Mg_{0.1}O_{2.9}$ (open triangle).

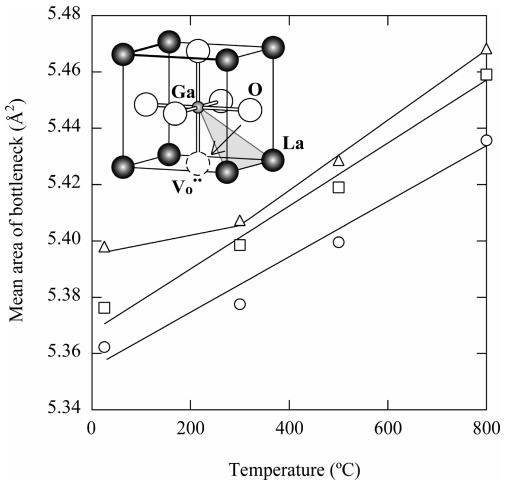

Figure 11. Mean areas of bottlenecks of $LaGaO_3$ (open circle), $LaGa_{0.9}Mg_{0.1}O_{2.95}$ (open square), and $La_{0.9}Sr_{0.1}Ga_{0.9}Mg_{0.1}O_{2.9}$ (open triangle) as a function of temperature. Inset shows structural model that the oxide ion passes though the bottleneck (shown by triangle) formed by two A-site cations and one B-site cation.

shown in Figure 10. It is, therefore, supposed that the oxide ion of LSGM9191 can easily move to the neighboring oxygen vacancy sites, corresponding to the lower conduction activation energy of LSGM9191.

Cook et al.[34] and Sammells et al.[35] reported that the oxide ion in the perovskite structure must pass through bottlenecks formed by two A-site cations and one B-site cation. The bottleneck is represented as a free area in the unit cell of the perovskite structure. Namely, it is considered that the larger bottleneck brought the high oxide ion conduction property. In addition, Slater et al.[15] reported that when the structure is undistorted, the oxide ion is easily able to pass through the bottleneck and when the structure is distorted, the oxide ion conduction pass is restricted. Figure 11 shows mean areas of bottlenecks in LG, LGM91, and LSGM9191 as a function of temperature. The mean areas of bottlenecks were increased with temperature. The mean areas of bottlenecks in LSGM9191 became larger than those in LGM91 by doping Sr in LGM91. The larger areas of bottlenecks and the significant reduction of the GaO_6 octahedral tilts in LSGM9191 led the oxide ion conduction property to the enhancement. As a result, oxide ion conductivity of LSGM9191 was higher than that of LGM91. It is considered that this is consistent with the anisotropic distribution of oxygen atom in LSGM9191 at 500 and 800 °C being larger than that in LGM91.

Further structural analyses of $LaGaO_3$-based materials with the same oxygen vacancies concentration, e.g., $LaGa_{0.8}Mg_{0.2}O_{2.9}$ and $La_{0.9}Sr_{0.1}Ga_{0.9}Mg_{0.1}O_{2.9}$, are in progress in order to comprehend the conduction mechanism in these systems.

Conclusions

We have investigated crystal structures and oxide ion conduction properties of $LaGaO_3$-based perovskite compounds by high-temperature neutron powder diffraction and oxide ion conductivity measurement, respectively. The

(34) Cook, R. L.; Sammells, A. F. *Solid State Ionics* **1991**, *45*, 311.
(35) Sammells, A. F.; Cook, R. L.; White, J. H.; Osborne, J. J.; MacDuff, R. C. *Solid State Ionics* **1992**, *52*, 111.

doping Sr and Mg significantly affected the symmetry of low-temperature phases of $LaGaO_3$-based perovskite, and furthermore made the transition temperature rise. Namely, $LaGaO_3$ parent phase crystallized in the orthorhombic (*Pbnm*) at room temperature and the rhombohedral ($R\bar{3}c$) at between 160 and 800 °C. $LaGa_{0.9}Mg_{0.1}O_{2.95}$ crystallized in the orthorhombic (*Ibmm*) up to 340 °C and the rhombohedral ($R\bar{3}c$) at between 350 and 800 °C. On the other hand, $La_{0.9}Sr_{0.1}Ga_{0.9}Mg_{0.1}O_{2.9}$ crystallized in the monoclinic ($I2/a$) up to 400 °C and the rhombohedral ($R\bar{3}c$) in the temperature range of 410−800 °C.

The GaO_6 octahedral tilts were observed in all the samples, and the doping Sr and Mg led the GaO_6 octahedral tilts to the reduction. Particularly, the doping Sr in $LaGa_{0.9}Mg_{0.1}O_{2.95}$ was significantly effective for reduction of the GaO_6 octahedral tilts. In addition, the areas of bottlenecks in $La_{0.9}Sr_{0.1}Ga_{0.9}Mg_{0.1}O_{2.9}$ were larger than those of $LaGa_{0.9}Mg_{0.1}O_{2.95}$ and the oxide ion conductivity of the former was higher than that of the latter.

Consequently, the large areas of bottleneck and the reduction of GaO_6 octahedral tilts in $La_{0.9}Sr_{0.1}Ga_{0.9}Mg_{0.1}O_{2.9}$ were found to result in the enhancement of the oxide ion conduction property. This result supports larger anisotropy of oxide ions in $La_{0.9}Sr_{0.1}Ga_{0.9}Mg_{0.1}O_{2.9}$.

Acknowledgment. M.K. thanks the Japan Society for the Promotion of Science (JSPS) for its financial support to start this study. This work was also funded in part by a Grant-in-Aid for Scientific Research (B) (16360331) from JSPS and the Okayama University 21st Century COE Program “Strategic Solid Waste Management of Sustainable Society”.

CM050597N